

Ephrin-B2 regulates VEGFR2 function in developmental and tumour angiogenesis

Suphansa Sawamiphak¹, Sascha Seidel², Clara L. Essmann¹, George A. Wilkinson³, Mara E. Pitulescu⁴, Till Acker^{2*} & Amparo Acker-Palmer^{1*}

The formation and guidance of specialized endothelial tip cells is essential for both developmental and pathological angiogenesis¹. Notch-1 signalling regulates the generation of tip cells, which respond to gradients of vascular endothelial growth factor (VEGF-A)². The molecular cues and signalling pathways that control the guidance of tip cells are poorly understood. Bidirectional signalling by Eph receptors and ephrin ligands represents one of the most important guidance cues involved in axon path finding³. Here we show that ephrin-B2 reverse signalling involving PDZ interactions regulates endothelial tip cell guidance to control angiogenic sprouting and branching in physiological and pathological angiogenesis. *In vivo*, ephrin-B2 PDZ-signalling-deficient mice (ephrin-B2ΔV) exhibit a reduced number of tip cells with fewer filopodial extensions at the vascular front in the mouse retina. In pathological settings, impaired PDZ signalling decreases tumour vascularization and growth. Mechanistically, we show that ephrin-B2 controls VEGF receptor (VEGFR)-2 internalization and signalling. Importantly, internalization of VEGFR2 is necessary for activation and downstream signalling of the receptor and is required for VEGF-induced tip cell filopodial extension. Together, our results suggest that ephrin-B2 at the tip cell filopodia regulates the proper spatial activation of VEGFR2 endocytosis and signalling to direct filopodial extension. Blocking ephrin-B2 reverse signalling may be an attractive alternative or combinatorial anti-angiogenic therapy strategy to disrupt VEGFR2 function in tumour angiogenesis.

Vessels and nerves possess similar specialized structures—tip cells and growth cones—that, through filopodial extensions, sense the surrounding tissue for specific cues that direct their movements. Emerging evidence suggests that axonal growth cones and capillary tip cells use common repulsive and attractive signals in their environment that ultimately determine their directional guidance through the body^{4,5}. Indeed, axon guidance molecules such as netrins, semaphorins, slits and ephrins are essential for normal vascular patterning^{5,6} and therefore might mediate guidance events controlling vascular sprouting. Ephrin-B2, a transmembrane ligand for Eph receptors, possesses intrinsic signalling capabilities that are required for early angiogenic remodelling^{7–9}. However, the molecular mechanism underlying the function of ephrin-B2 in coordinating proper development and function of the vasculature is currently unknown. Because ephrinB ligands have well-defined functions as repulsive molecules for the guidance of axons, we investigated whether ephrin-B2 would have a role in tip-cell guidance and function.

To study the role of ephrin-B2 reverse signalling during angiogenesis *in vivo*, we used two different mouse lines with either a targeted

mutation of five tyrosine residues (ephrin-B25Y) or a deletion of a single valine residue in the cytoplasmic domain of ephrin-B2 (ephrin-B2ΔV), which impair phosphotyrosine- or PDZ-dependent reverse signalling, respectively. The latter is required for the remodelling of the lymphatic vasculature¹⁰ as well as postnatal lung alveolar development¹¹. We first focused on the function of ephrin-B2 in developmental angiogenesis by investigating angiogenic sprouting in the mouse retina¹². Extension of the developing superficial vascular plexus was impaired in the newborn ephrin-B2ΔV mice compared with wild-type littermates and ephrin-B25Y mice (Fig. 1a–c and Supplementary Fig. 1a). Ephrin-B2ΔV, but not ephrin-B25Y, P7 retinas showed a 25% decrease in vessel branching and a striking reduction in the number of vascular sprouts quantified by the number of filopodial bursts in the developing vascular plexus (Supplementary Fig. 1b–i). The vascularization of different brain regions such as cortex, thalamus and striatum as well as retina was similarly reduced by more than 20% in ephrin-B2ΔV adult mice (Supplementary Fig. 1j–l). Detailed analysis of the vascular front revealed that filopodial density was strikingly reduced (56.7% reduction in the number of filopodia per vessel length in ephrin-B2ΔV mice compared with control littermates) (Fig. 1d, e), whereas proliferation at the vascular front was not affected (Supplementary Fig. 2), suggesting that reduced sprouting activity rather than endothelial proliferation accounted for the reduced vessel density. In agreement with a function of ephrin-B2 at the tip cell, ephrin-B2 clusters localized to tip cell filopodia (Fig. 1f). During retinal development an astrocyte scaffold guides the extension of tip cell filopodia and the subsequent migration of endothelial sprouts^{13–16}. Interestingly, EphB receptors are abundantly expressed in retinal astrocytes (Supplementary Fig. 3) and might, with EphB receptors expressed in retinal endothelial cells (see accompanying paper¹⁷), represent a source of activation of ephrin-B2 clusters at the tip cell. Conditional strategies to remove EphB receptors from these tissues specifically by cell type will help to address their relative contributions to the activation of ephrin-B2 at the tip cell. Gain-of-function experiments revealed a direct effect of ephrin-B2 on filopodial extension dynamics in endothelial cells (Fig. 1g–j and Supplementary Movie 1). This excessive extension of filopodia prevented inclusion of endothelial cells into tubular structures (Supplementary Fig. 4 and Supplementary Movie 2) and was dependent on reverse ephrin-B2 PDZ signalling (Supplementary Fig. 4, Supplementary Fig. 5 and Supplementary Movies 2–6). These observations are consistent with an intercellular repulsive activity regulated by Eph-ephrin contacts^{18,19} that might, for example, set off the initial destabilizing forces needed for the budding of the selected sprouting endothelial cell (tip

¹Frankfurt Institute for Molecular Life Sciences and Institute of Cell Biology and Neuroscience, Goethe University Frankfurt, Max-von-Laue-Strasse 9, D-60438 Frankfurt am Main, Germany. ²Institute of Neuropathology, Giessen University, Arndtstrasse 16, D-35392 Giessen, Germany. ³Developmental Vascular Biology Program, Medical College of Wisconsin, 8701 Watertown Plank Road, Milwaukee, Wisconsin 53226, USA. ⁴Department of Tissue Morphogenesis, Max-Planck-Institute for Molecular Biomedicine, and Faculty of Medicine, University of Münster, Röntgenstrasse 20, D-48149 Münster, Germany.

*These authors contributed equally to this work.

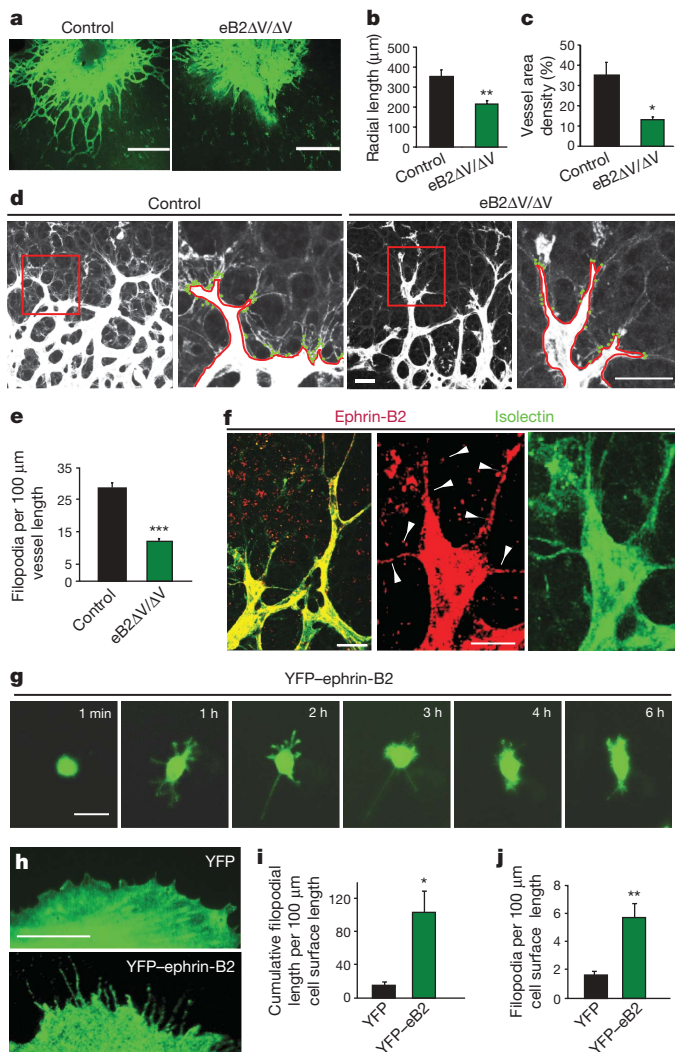


Figure 1 | Ephrin-B2 PDZ interactions are required *in vivo* for tip cell filopodial extension during developmental angiogenesis. **a**, Isolectin-B4 staining of control and ephrin-B2 $\Delta V/\Delta V$ P1 retinas. **b**, **c**, Quantification based on radial length from optic nerve to the periphery (**b**) and on the percentage of retina area covered with vessels (**c**) (s.e.m., $n = 6-8$). **d**, **e**, Ephrin-B2 ΔV mice exhibit reduced filopodial extensions (green dots) per vessel length (red line) at the sprouting front as quantified in **e** (s.e.m., $n = 10-12$). **f**, Retinal whole-mount staining with EphB4-Fc shows ephrin-B2 clusters at the tip cell filopodia (white arrows). **g-j**, Ephrin-B2 induces filopodial extensions in MECs. Six frames of Supplementary Movie 1 (**g**) and higher magnification of the cell surface (**h**) are shown. Cumulative filopodial length (**i**) and number of filopodia (**j**) per 100 μm of cell surface length are quantified (s.e.m., $n = 14$). Scale bars, 150 μm (**a**), 100 μm (**d**, higher magnifications), 25 μm (**d**, **f** left panel, **g**, **h**) and 10 μm (**f**, middle panel). * $P < 0.05$, ** $P < 0.01$, *** $P < 0.001$.

cell) from a quiescent tube. Together, our results indicate that ephrin-B2 reverse signalling through PDZ interactions controls vessel sprouting by promoting tip cell filopodial extension during developmental angiogenesis.

VEGF is a crucial regulator during the initial establishment of astrocyte-endothelial interactions that mediate endothelial cell guidance along the pre-existing astrocytic scaffold^{13,20}. Therefore, we next investigated if the lack of filopodial extensions in ephrin-B2 ΔV tip cells could be a result of misregulated VEGF receptor function indicating a molecular crosstalk between ephrin-B2 reverse and VEGFR signalling. The tight regulation of intracellular VEGFR2 localization is an important mechanism to control its signalling properties²¹. At the cellular surface VEGFR2 is dephosphorylated and inactivated by the action of membrane-associated phosphatases such as CD148 (ref. 22)

or VE-PTP²³. Conversely, internalization of VEGFR2, as for TGF- β , EGF or NGF receptors, promotes signalling in the endosomal compartment^{22,24}. Indeed, ephrin-B2 PDZ interactions were required for VEGF-induced internalization of VEGFR2 in endothelial cells (Fig. 2a, b), supporting our *in vivo* findings of an exclusive requirement of PDZ interactions downstream of ephrin-B2 ligands for proper vessel sprouting (Fig. 1). Total VEGFR2 and ephrin-B2 expression levels were not changed in ephrin-B2 ΔV compared with control cells (Supplementary Fig. 6). To corroborate functionally the control of VEGFR2 endocytosis by ephrin-B2 reverse signalling we

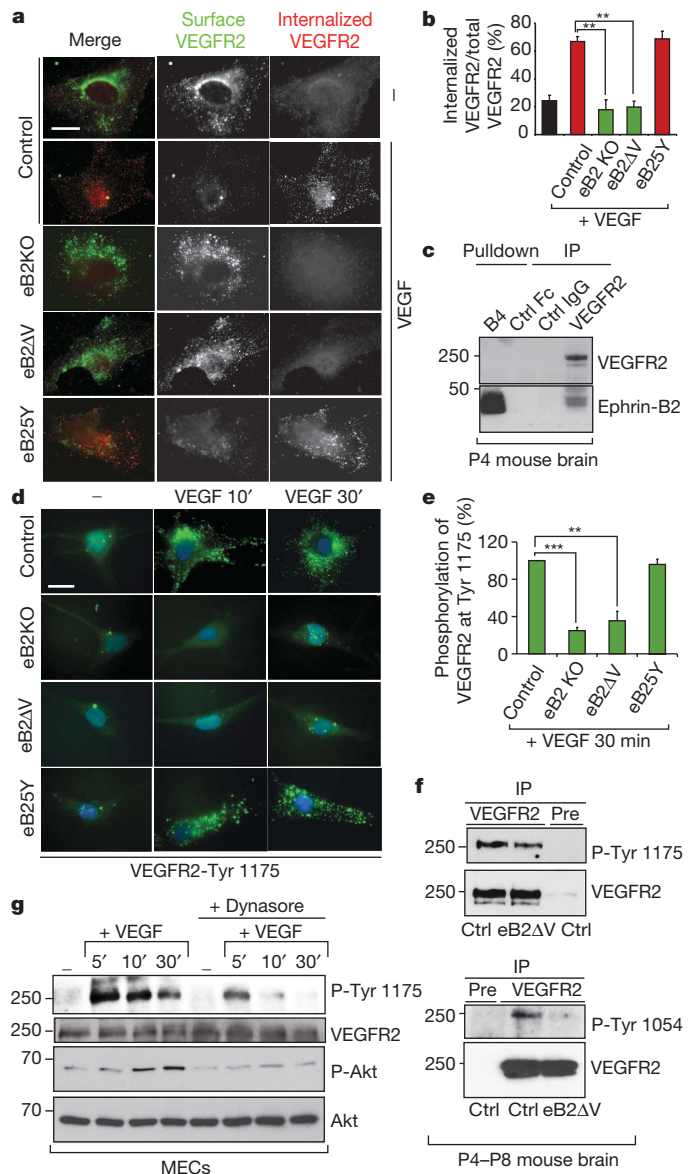


Figure 2 | Ephrin-B2 controls VEGFR2 internalization and signalling. **a**, **b**, Endocytosis of VEGFR2 visualized by an 'antibody feeding' assay (see Methods) in MECs stimulated for 30 min with VEGF and quantified based on fluorescence intensities (s.e.m., $n \geq 20$). **c**, VEGFR2 co-precipitates with ephrin-B2. As a reference ephrin-B2 was pulled down with EphB4-Fc. **d**, **e**, VEGFR2-Tyr 1175 phosphorylation in MECs. Quantification is shown as the percentage of fluorescence in every mutant versus total intensity in controls after 30 min VEGF treatment (**e**) (s.e.m., $n \geq 24$). **f**, VEGFR2 phosphorylation *in vivo* on Tyr 1175 and Tyr 1054 is compromised in ephrin-B2 ΔV mouse mutants. Ctrl, control. **g**, Internalization of VEGFR2 is necessary for activation of the receptor and downstream signalling. VEGF-induced phosphorylation on VEGFR2-Tyr 1175 and Akt in MECs untreated or pre-treated for 2 h with dynasore is shown. Scale bar, 25 μm . ** $P < 0.01$, *** $P < 0.001$.

next stimulated endothelial cells with soluble EphB4 receptor to activate ephrin-B2 reverse signalling^{25,26}. Activation of ephrin-B2 was sufficient to induce VEGFR2 internalization and, like VEGF-mediated internalization of VEGFR2, EphB4-induced VEGFR2 internalization required a functional PDZ target site on ephrin-B2 (Supplementary Fig. 7a, b). EphB4-induced internalization of VEGFR2 was confirmed in a biotinylation assay with endothelial cells and live mouse tissue (Supplementary Fig. 7c, d). Activation of ephrin-B2 specifically induced the internalization of VEGFR2 but not other angiogenic receptors such as Tie2. Importantly, internalization of VEGFR2 but not Tie2 was impaired in ephrin-B2ΔV mice (Supplementary Fig. 7c, d). In line with a direct control of VEGFR2 endocytosis by ephrin-B2, VEGFR2 co-localized with surface ephrin-B2 ligand patches (Supplementary Fig. 8) and both proteins co-immunoprecipitated (Fig. 2c). Together, our results indicate that ephrin-B2, through PDZ interactions, is a potent regulator of VEGFR2 trafficking.

To address whether the regulation of VEGFR2 trafficking by ephrinB reverse signalling influences VEGFR2 activation, we assessed VEGFR2 tyrosine phosphorylation and downstream signalling. In agreement with the control of VEGFR2 internalization by ephrin-B2 reverse signalling, ephrin-B2 knockout and ephrin-B2ΔV endothelial cells displayed a striking reduction in VEGFR2 phosphorylation whereas ephrin-B25Y cells did not show any defects (Fig. 2d, e). Correspondingly, *in vivo*, ephrin-B2ΔV mice showed reduced levels of VEGFR2 phosphorylation at different phosphorylation sites (Fig. 2f and Supplementary Fig. 9a), suggesting that ephrin-B2ΔV mice fail to internalize and activate VEGFR2 efficiently. VEGF-induced Akt activation was impaired in ephrin-B2ΔV endothelial cells (Supplementary Fig. 9b). The requirement of VEGFR2 internalization for signalling was confirmed using dynasore, a potent inhibitor of dynamin-dependent endocytic pathways²⁷. Treatment of endothelial cells with dynasore inhibited VEGF-induced VEGFR2 phosphorylation and downstream signalling assessed by Akt activation (Fig. 2g and Supplementary Fig. 10). To prove that VEGFR2 internalization is functionally required for tip cell filopodial extension, we developed a short-term culture system of explanted retinas that allowed us to stimulate the tissue acutely and to assess cellular responses of tip cells at the vascular front. These explanted retinas robustly responded to stimulation with VEGF-A, as evidenced by the increased number of filopodial extensions per vessel length (Fig. 3a, b). Co-treatment with dynasore impaired filopodial extension, indicating the requirement for VEGFR2 internalization to induce tip cell function. The ability of activated ephrin-B2 to induce filopodial extension directly in endothelial cells (Fig. 1g, j) was confirmed in the tissue by stimulating retinal explants with EphB4-Fc. Activation of ephrin-B2 was sufficient to increase the number of filopodial extensions in tip cells significantly (Fig. 3c, d). To underline the role of ephrin-B2 as a potent regulator of VEGFR2 internalization and function, we acutely deprived the retinal explants of VEGF-A by applying a soluble VEGFR1 extracellular domain-Fc fusion protein (soluble Flt-1), which binds VEGF-A with high affinity and has been used extensively as a VEGF-A trap¹³. Filopodial extension was severely compromised after sFlt-1 treatment but was significantly rescued when ephrin-B2 was simultaneously activated by EphB4-Fc treatment (Fig. 3c, d), suggesting that ephrin-B2 functionally cooperates with VEGF to stimulate VEGFR2 at the tip cell. In summary, we propose a model of ephrin-B2 function at the tip cell where activation of ephrin-B2 induces VEGFR2 internalization and activation, thereby controlling tip cell filopodial extension and vascular sprouting (Fig. 3e).

Because our data identified ephrin-B2 reverse signalling as a potent regulator of VEGFR2 function, we next explored if ephrin-B2 reverse signalling also controls VEGFR2 function during tumour angiogenesis. We first assessed intracranial tumour growth in ephrin-B2ΔV mice using an orthotopic glioma tumour model²⁸ (see Methods). Intracranial tumour growth in ephrin-B2ΔV mice was severely reduced, reaching less than 25% of the volume of control tumours

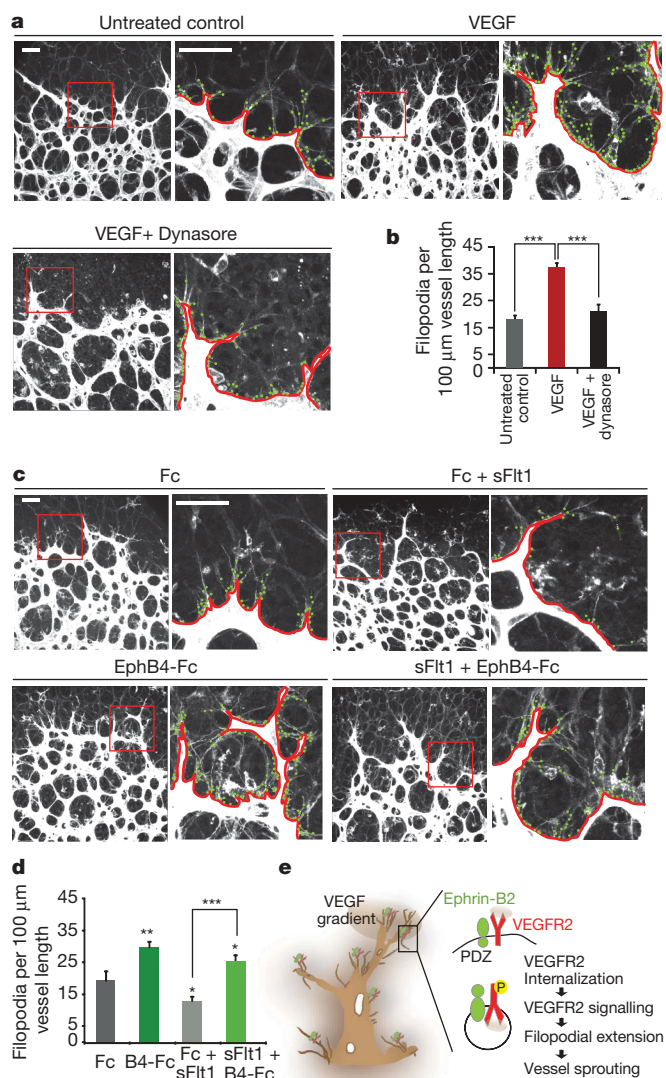


Figure 3 | Ephrin-B2-mediated VEGFR2 internalization is required for tip cell filopodial extension. **a, b**, VEGF-induced tip cell filopodial extension requires internalization of VEGFR2. P4 retinal explants stimulated with VEGF-A or with VEGF-A and dynasore for 4 h. Filopodial extension analysed and quantified as in Fig. 1b (**b**) (s.e.m., $n = 14-19$). **c, d**, Activation of ephrin-B2 induces tip cell filopodial extension and rescues tip cell filopodial dynamics after VEGF sequestering. P4 retinal explants stimulated with Fc, EphB4-Fc, Fc and soluble Flt-1, or soluble Flt-1 and EphB4-Fc for 4 h. Filopodial extensions analysed and quantified as above (**d**) (s.e.m., $n = 11-15$). **e**, Model of ephrin-B2 function at the tip cell filopodia. Ephrin-B2 (green) expressed at the tip cell filopodia regulates VEGFR2 (red) internalization and signalling to control filopodial extension and vessel sprouting. Line represents plasma membrane and circle endocytic vesicle. Scale bar, 25 μm. * $P < 0.05$, ** $P < 0.01$, *** $P < 0.001$.

in wild-type littermates (Fig. 4a, b). The stunted tumour growth was associated with a decreased tumour vascularization, as reflected by the quantification of the vascular area density (Fig. 4c, d). Quantification of vessel perfusion (marked by intravascular lectin) revealed a similar decrease in functional vascular area (data not shown). Morphologically, the vasculature of control tumours consisted of tortuous and highly branched blood vessels (Fig. 4c). Vascular sprouts and filopodial extensions were readily detectable on the blood vessels of control tumours (Fig. 4c, higher magnifications). In contrast, the vasculature of the tumours grown in ephrin-B2ΔV mice was less tortuous and less branched (Fig. 4c). Importantly, like the reduction in vascular sprouting seen in retinal vascularization after impaired PDZ-dependent signalling (Fig. 1a-e

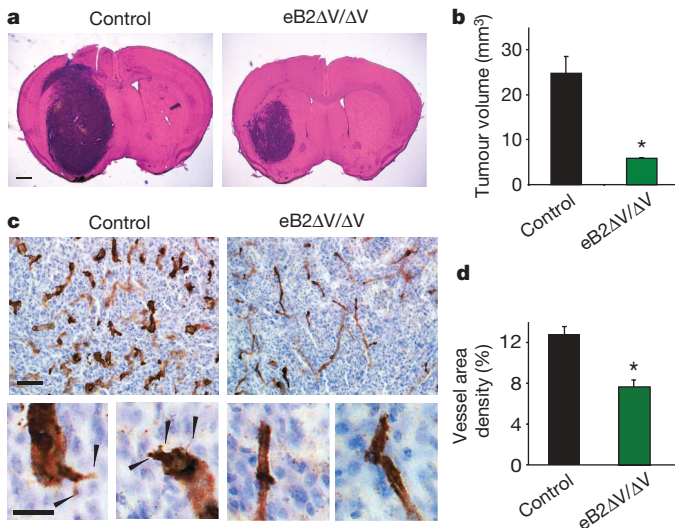


Figure 4 | Ephrin-B2 PDZ interactions control tip cell filopodial dynamics during tumour angiogenesis. **a, b**, Intracranial astrocytoma growth is reduced in ephrin-B2ΔV (eB2 ΔV/ΔV) mice compared with control littermates. Tumours were stained with haematoxylin and eosin (HE) (s.e.m., $n = 7-11$). **c, d**, Vessel density, assessed with CD34 staining, is decreased in astrocytomas grown in ephrin-B2ΔV mice compared with control littermates. Higher magnification images are shown at the bottom panels (**c**). Arrowheads point to filopodial extensions in the tumour vessels. Note the smooth and normalized vessels in the ephrin-B2ΔV mutants. Quantification of vessel density is based on the area covered by vessel staining (**d**) (s.e.m., $n = 7-11$). Scale bars, 1 mm (**a**), 100 μm (**c**), 25 μm (higher magnifications in **c**). * $P < 0.05$, *** $P < 0.001$.

and Supplementary Fig. 1), the tumour blood vessels in ephrin-B2ΔV mice were devoid of sprouts and filopodia (Fig. 4c, higher magnifications), indicating that ephrin-B2 reverse signalling controls VEGFR2 function in tumour vessels. Interestingly, this phenotype was not restricted to the brain vasculature as reduction in tumour growth and vascularization were reproduced in a heterotopic tumour model in the skin of ephrin-B2ΔV mice (Supplementary Fig. 11). Moreover, we confirmed that the function of ephrin-B2 during pathological angiogenesis is endothelial specific because comparable tumour and vascular phenotypes were observed in GL261 astrocytomas injected in mice with an endothelial-specific tamoxifen-inducible ephrin-B2 loss-of-function (ephrin-B2^{ΔE/C}; for description of the mice see Methods and the accompanying paper¹⁷) (Supplementary Fig. 12).

Together, our results identify ephrin-B2 reverse signalling through PDZ interactions as a positive regulator of VEGFR2 trafficking and signalling to control endothelial tip-cell-mediated vessel sprouting in physiological and pathological settings. Directional migration guided by surface receptors has been shown to be tightly regulated by RTK endocytosis, which ensures localized intracellular responses to guidance cues by stimulating spatial restriction of signalling. These effects have been extensively studied in border cells that perform a stereotypic migration during oogenesis in *Drosophila*²⁹. Our results reinforce such a model for RTK guidance during vascular sprouting events. We postulate that ephrin-B2 activation at the tip cell filopodia regulates proper spatial activation of VEGFR2 by controlling receptor endocytosis. Interestingly, our observation of nude vascular structures devoid of sprouts and filopodia in the tumours grown in ephrin-B2ΔV mice indicates a general mechanism for ephrin-B2 in regulating VEGFR2 action both in physiological and pathological angiogenesis. Moreover, the function of ephrin-B2 ligands in the regulation of VEGFR trafficking seems to extend beyond VEGFR2 and to include other family members such as VEGFR3 (see accompanying paper¹⁷). Importantly, VEGFR3 has recently been shown to be localized prominently at the filopodial extensions of tip cells,

acting as a modulator of developmental and pathological angiogenesis³⁰. It has subsequently been proposed that a combination of VEGF/VEGFR2 and VEGFR3 blockade may improve the outcome of anti-VEGF therapies³¹. Thus, blocking ephrin-B2 signalling in tumours might represent an intriguing strategy to interfere simultaneously with both VEGFR2 and VEGFR3 function that could be used as an alternative or combinatorial anti-angiogenic treatment for tumour therapy.

METHODS SUMMARY

Endothelial cell culture. Primary mouse endothelial cells (MECs) from P4-7 ephrin-B2^{lox/lox} mice were isolated from lung with collagenase treatment and purified by CD31-coupled magnetic beads. Ephrin-B2 knockout endothelial cells were generated by Cre recombinase adenoviral infection (Vector Biolabs).

Retinal vasculature analysis. Mouse retinas were dissected and retinal vessels were visualized as described in the Methods. Images were acquired using a confocal microscope (Leica TCS SP2). Quantitative measurements were performed using ImageJ (National Institutes of Health) and MetaMorph (Molecular Devices).

Acute retinal explants. Retinas were dissected from P4-5 pups and flat-mounted onto hydrophilic membrane filters (40 μm pore size) as described in the Methods. Retina explants were incubated in a humidified incubator supplied with 5% CO₂ for 2-4 h for recovery before stimulation.

Antibody feeding assay. Antibody feeding assays were performed as described²⁶. Images were acquired using a digital camera (SpotRT; Diagnostic Instruments) attached to an epifluorescence microscope (Zeiss) equipped with a ×63 objective (Plan-Apochromat, Zeiss). All quantitative measurements were performed using MetaMorph software (Molecular Devices).

Astrocytoma generation and tumour injections. Murine astrocytomas were generated as described²⁸. Astrocytes isolated from perinatal mice were immortalized by transfection with SV40 large T-antigen and transformed to astrocytomas by viral transduction of H-rasV12 (pBabe puro H-Ras V12, Addgene). Tumour cells were injected stereotactically into the left striatum or subcutaneously in ephrin-B2ΔV mice or control littermates. To avoid immune rejection, mice from the same crossing generation were used for astrocyte isolation and tumour injection. GL261 astrocytoma cells were injected stereotactically in the left striatum of ephrin-B2^{ΔE/C} mice. All the animal experiments were conducted under institutional guidelines and were approved by the Hessen Animal Ethics Committees.

Full Methods and any associated references are available in the online version of the paper at www.nature.com/nature.

Received 24 October 2009; accepted 2 March 2010.

Published online 5 May 2010.

- Carmeliet, P. Angiogenesis in life, disease and medicine. *Nature* **438**, 932-936 (2005).
- Phng, L. K. & Gerhardt, H. Angiogenesis: a team effort coordinated by notch. *Dev. Cell* **16**, 196-208 (2009).
- Egea, J. & Klein, R. Bidirectional Eph-ephrin signaling during axon guidance. *Trends Cell Biol.* **17**, 230-238 (2007).
- Lu, X. *et al.* The netrin receptor UNC5B mediates guidance events controlling morphogenesis of the vascular system. *Nature* **432**, 179-186 (2004).
- Larrivee, B. *et al.* Guidance of vascular development: lessons from the nervous system. *Circ. Res.* **104**, 428-441 (2009).
- Adams, R. H. & Alitalo, K. Molecular regulation of angiogenesis and lymphangiogenesis. *Nature Rev. Mol. Cell Biol.* **8**, 464-478 (2007).
- Pasquale, E. B. Eph-ephrin bidirectional signaling in physiology and disease. *Cell* **133**, 38-52 (2008).
- Adams, R. H. *et al.* Roles of ephrinB ligands and EphB receptors in cardiovascular development: demarcation of arterial/venous domains, vascular morphogenesis, and sprouting angiogenesis. *Genes Dev.* **13**, 295-306 (1999).
- Adams, R. H. *et al.* The cytoplasmic domain of the ligand ephrinB2 is required for vascular morphogenesis but not cranial neural crest migration. *Cell* **104**, 57-69 (2001).
- Makinen, T. *et al.* PDZ interaction site in ephrinB2 is required for the remodeling of lymphatic vasculature. *Genes Dev.* **19**, 397-410 (2005).
- Wilkinson, G. A. *et al.* Role for ephrinB2 in postnatal lung alveolar development and elastic matrix integrity. *Dev. Dyn.* **237**, 2220-2234 (2008).
- Gariano, R. F. & Gardner, T. W. Retinal angiogenesis in development and disease. *Nature* **438**, 960-966 (2005).
- Gerhardt, H. *et al.* VEGF guides angiogenic sprouting utilizing endothelial tip cell filopodia. *J. Cell Biol.* **161**, 1163-1177 (2003).
- Watanabe, T. & Raff, M. C. Retinal astrocytes are immigrants from the optic nerve. *Nature* **332**, 834-837 (1988).

15. Gariano, R. F. *et al.* Development of astrocytes and their relation to blood vessels in fetal monkey retina. *Invest. Ophthalmol. Vis. Sci.* **37**, 2367–2375 (1996).
16. Dorrell, M. I. *et al.* Retinal vascular development is mediated by endothelial filopodia, a preexisting astrocytic template and specific R-cadherin adhesion. *Invest. Ophthalmol. Vis. Sci.* **43**, 3500–3510 (2002).
17. Wang, Y. *et al.* Ephrin-B2 controls VEGF-induced angiogenesis and lymphangiogenesis. *Nature* doi:10.1038/nature09002 (this issue).
18. Mellitzer, G. *et al.* Eph receptors and ephrins restrict cell intermingling and communication. *Nature* **400**, 77–81 (1999).
19. Zimmer, M. *et al.* EphB-ephrinB bi-directional endocytosis terminates adhesion allowing contact mediated repulsion. *Nature Cell Biol.* **5**, 869–878 (2003).
20. Dorrell, M. I. & Friedlander, M. Mechanisms of endothelial cell guidance and vascular patterning in the developing mouse retina. *Prog. Retin. Eye Res.* **25**, 277–295 (2006).
21. Bhattacharya, R. *et al.* Regulatory role of dynamin-2 in VEGFR-2/KDR-mediated endothelial signaling. *FASEB J.* **19**, 1692–1694 (2005).
22. Lampugnani, M. G. *et al.* Vascular endothelial cadherin controls VEGFR-2 internalization and signaling from intracellular compartments. *J. Cell Biol.* **174**, 593–604 (2006).
23. Mellberg, S. *et al.* Transcriptional profiling reveals a critical role for tyrosine phosphatase VE-PTP in regulation of VEGFR2 activity and endothelial cell morphogenesis. *FASEB J.* **23**, 1490–1502 (2009).
24. Lee, S. *et al.* Autocrine VEGF signaling is required for vascular homeostasis. *Cell* **130**, 691–703 (2007).
25. Palmer, A. *et al.* EphrinB phosphorylation and reverse signaling: regulation by Src kinases and PTP-BL phosphatase. *Mol. Cell* **9**, 725–737 (2002).
26. Essmann, C. L. *et al.* Serine phosphorylation of ephrinB2 regulates trafficking of synaptic AMPA receptors. *Nature Neurosci.* **11**, 1035–1043 (2008).
27. Macia, E. *et al.* Dynasore, a cell-permeable inhibitor of dynamin. *Dev. Cell* **10**, 839–850 (2006).
28. Blouw, B. *et al.* The hypoxic response of tumors is dependent on their microenvironment. *Cancer Cell* **4**, 133–146 (2003).
29. Jekely, G. *et al.* Regulators of endocytosis maintain localized receptor tyrosine kinase signaling in guided migration. *Dev. Cell* **9**, 197–207 (2005).
30. Tammela, T. *et al.* Blocking VEGFR-3 suppresses angiogenic sprouting and vascular network formation. *Nature* **454**, 656–660 (2008).
31. Padera, T. P. & Jain, R. K. VEGFR3: a new target for antiangiogenesis therapy? *Dev. Cell* **15**, 178–179 (2008).

Supplementary Information is linked to the online version of the paper at www.nature.com/nature.

Acknowledgements We thank R. Klein for the ephrin-B2^{lox/lox} mice, A. Filosa, F. Finkelmeier and H. zum Buttel for technical support, A. Filosa and B. Garvalov for comments on the manuscript and R. Adams for scientific input and reading the manuscript. We acknowledge the Max Planck Institute of Neurobiology in Martinsried (Germany) and the Edinger Institute at Frankfurt University (Germany) for support and the use of equipment and animal facilities in the early stages of this project. This work was supported by grants from the Deutsche Forschungsgemeinschaft within the SPP1190 (AC110/3-1, 3-2 to T.A. and AC180/3-1, 3-2 to A.A.-P.), the Deutsche Krebshilfe (107231 to T.A.) and the Clusters of Excellence 'Macromolecular Complexes (CEF)' (EXC 115) at the University Frankfurt and 'Cardio-Pulmonary System (ECCPS)' (EXC 147) at the Universities of Giessen and Frankfurt.

Author Contributions S.Sa. designed experiments and performed all the characterization of developmental angiogenesis of the mice, the retinal explant cultures, time lapse experiments, antibody feeding assays, part of the biochemistry and generated the astrocytomas for the tumour angiogenesis part. S.Se. performed the tumour injections and the analysis of tumour growth and vasculature. C.L.E. performed most of the biochemistry. G.A.W. and M.E.P. generated mouse mutants. T.A. designed experiments, interpreted results in the tumour angiogenesis part and wrote the manuscript. A.A.-P. designed experiments and interpreted results in the developmental part, helped with quantifications, prepared all the figures and wrote the manuscript.

Author Information Reprints and permissions information is available at www.nature.com/reprints. The authors declare no competing financial interests. Correspondence and requests for materials should be addressed to A.A.-P. (Acker-Palmer@bio.uni-frankfurt.de).

METHODS

Mouse mutants

Primary endothelial cell isolation. The generation of the conditional knockout mice ephrin-B2^{lox/lox} has been described³². Ephrin-B2^{ΔV/ΔV} and ephrin-B2^{5Y/5Y} mice have been generated as described¹⁰. P4–7 mice were killed. Lungs were removed into dissection buffer (HBSS, Gibco, supplemented with 10% fetal bovine serum, Hyclone) and minced into small pieces. The tissues were then treated with equal volumes of collagenase type II (Biochrom, 260 units per millilitre) at 37 °C in a humidified incubator supplied with 5% CO₂ for 30 min with occasional shaking. The mixtures were passed through 40 μm disposable cell strainer and centrifuged at 200g for 5 min at 4 °C. Lung tissue pellets were collected and resuspended in dissection buffer. Tissue suspensions were centrifuged at 200g for 5 min at 4 °C and pellets were collected and resuspended twice in fresh dissection buffer to wash out remaining collagenase. After washing, tissue pellets were resuspended in 2 ml dissection buffer and incubated with anti-rat IgG coated magnetic beads (Invitrogen, 8 × 10⁷ beads per lung) pre-coupled with rat anti-mouse PECAM-1 (MEC13.3, BD Pharmingen, 7 μg per lung) at 4 °C for 1 h with gentle rotation. The beads were washed five times by placing the tube on a magnet (Invitrogen), aspirating the supernatant and refilling with dissection buffer. The washed beads were resuspended in endothelial cell medium consisting of DMEM + GlutaMAX-I + 4.5 mg l⁻¹ D-glucose (Gibco), 100 U ml⁻¹ penicillin, 100 μg ml⁻¹ streptomycin (PAA Laboratories), 20% fetal bovine serum which was previously tested not to promote cell differentiation (Hyclone) and 0.4% (v/v) endothelial cell growth supplement with heparin (Promocell), and plated onto gelatin-coated plates. The magnetic beads were detached from the cells by trypsinization in the first passage.

Generation of ephrin-B2 knockout endothelial cells and tube formation assays. Endothelial cells isolated from ephrin-B2^{lox/lox} mice were infected with adenovirus encoding Cre recombinase (Vector Biolabs). The virally infected cells were cultured for 1 week and tested for the lack of ephrin-B2 protein by immunofluorescence using EphB4-Fc and anti-Fc antibodies (Supplementary Fig. 5). Endothelial cells in sparse culture were detached with accutase (PAA), resuspended in starving medium containing DMEM + GlutaMAX-I + 4.5 mg l⁻¹ D-glucose (Gibco) and 1% fetal bovine serum (Hyclone), and plated onto 48-well plate pre-coated with Matrigel (BD Biosciences). Fifteen thousand cells were seeded per well. The plate was incubated at 37 °C in a humidified incubator supplied with 5% CO₂ for 6–8 h. Quantitative measurement of the tubular network based on the percentage of area covered with capillary structures was done by using ImageJ (National Institutes of Health) and MetaMorph software (Molecular Devices). Ephrin-B2KO cells were still able to form tubular structures although these tubes showed a 2.4-fold increase in tube disruption. However, ephrin-B2KO tubes were suitable for re-introduction of wild type and signalling mutants to study the repulsive activity conferred by ephrin-B2 signalling. For the time-lapse movies the percentages of non-integrated cells versus the total yellow fluorescent protein (YFP)-expressing cells identified at the beginning of each movie was quantified. At least three independent movies per condition were quantified.

Endothelial cell expression constructs, transfection and stimulation. The YFP-ephrin-B2 WT expression construct was generated as described³³. YFP-ephrin-B2ΔC (amino acids 1–167) was generated by replacing the CFP gene from pJK42 (CFP-ephrin-B2ΔC, provided by J. Lauterbach) with the YFP gene from pEYFP-N1 (Clontech) at the SalI and BsrGI cloning sites. To generate YFP-ephrin-B25Y, the BbsI-EcoRV fragment encoding the carboxy (C)-terminal part of ephrin-B2 in the YFP-ephrin-B2 plasmid was replaced by a fragment in which five conserved tyrosine residues of ephrin-B2 were mutated as previously described¹⁰. Generation of YFP-ephrin-B2ΔV was done by site-directed mutagenesis (Stratagene) to remove the C-terminal valine from the ephrin-B2 gene. The ephrin-B2 expression constructs were introduced into primary mouse endothelial cells by electroporation using basic endothelial Nucleofector Kit (Amaxa). Recombinant mouse EphB4-Fc and ephrin-B2-Fc chimaeras (R&D) pre-coupled with the antibody against human Fc (Jackson ImmunoResearch) at a final concentration of 4 μg ml⁻¹ were used for stimulation of the primary endothelial cells.

Analysis of postnatal retinal angiogenesis. Visualization of retinal vessels was done as described¹³ with minor modifications. Briefly, retinas dissected from neonatal mice (mutants or wild-type littermates as a control) were permeabilized and stained with 40 μg ml⁻¹ FITC conjugated lectin from *Bandeiraea simplicifolia* (Isolectin-B4, Sigma-Aldrich) at 4 °C overnight. After five washes with PBS, retinas were post-fixed in 4% paraformaldehyde (PFA) and flat mounted with Vectashield mounting medium containing 4',6-diamidino-2-phenylindole (DAPI) (Vector Laboratories). Quantification of retinal angiogenesis was done in P1 and P2 in a C57/BL6 background. For later stages (P7 and adult) all the quantification was done in the CD1 background because ephrin-B2ΔV mice in the C57/BL6

background die during the first week of life from a lymphatic phenotype. The numbers of branch points and filopodial bursts in arterial zones were quantified from randomly defined 30–35 microscopic fields from eight retinas per group for ephrin-B2ΔV and control littermates. The values were normalized with field sizes. Vascular density measurement was done by calculation of areas covered with vessels in at least five arterial zones in each retina using ImageJ. For the P2 C57/BL6 mouse retinas, the radial length of the vascular network was measured from the average length of at least three lines drawn from the centre of the retina in the optic disc to the edge of the network. Vascular density was measured from the vascular areas in 300 μm × 300 μm fields next to the optic discs. Six to eight retinas from each genotype were used for all quantifications. Filopodial protrusions at the vascular front were analysed from 20 microscopic fields picked from 10–12 retinas per group for ephrin-B2ΔV and control littermates and quantified using MetaMorph software (Molecular Devices). Student's *t*-tests were used to assess statistical significance of the differences between measurements.

Analysis of adult brain and retinal vasculature. Mice (mutants or wild-type littermates) were anaesthetized and 1.5 ml of 50 mg ml⁻¹ fluorescein isothiocyanate dextran, relative molecular mass 2 × 10⁶ (Sigma-Aldrich), in PBS were injected intracardially. Brains and eyes were dissected and fixed with 4% PFA at 4 °C overnight. Coronal brain sections (60 μm) were obtained with a vibratome and mounted with Vectashield mounting medium containing DAPI. Retinas were dissected and flat-mounted as described above. Confocal images of brain and retinal vessels were used to analyse vessel density based on areas of the brain or retinal tissues covered with vessels using ImageJ. Four mice from each genotype were used for quantifications and statistics using Student's *t* tests.

Acute retinal explants. Eyes were enucleated from new born pups (P4–5) and transferred to FBS-free DMEM medium. Retinas were dissected from eye cups and vitreous bodies were totally removed. Retinas were flat-mounted onto the hydrophilic polytetrafluoroethylene (PTFE) membrane of Millicell inserts (Millipore) with the photoreceptor layer on top and the nerve fibre layer attached to the membrane. DMEM with 10% FBS was layered underneath the membrane and dropped on retinas to prevent dryness. Retina explants were incubated at 35 °C in a humidified incubator with 5% CO₂ for 2–4 h before stimulation. For stimulation of retina endothelial tip cells, all factors diluted in DMEM with 3% FBS were layered underneath the insert membrane and dropped on the explants. Concentrations of VEGF164 and EphB4Fc or hFc used were 1 μg ml⁻¹ and 10 μg ml⁻¹, respectively. Soluble Flt-1 and dynasore were added to the medium at concentrations of 1 μg ml⁻¹ and 0.32 mM, respectively. Stimulation was performed at 35 °C in a humidified incubator with 5% CO₂ for 4 h. Explants were fixed with 4% PFA at 35 °C for 4 h and stained with isolectin-B4 as described above.

Antibody feeding assay. The assay was performed as described²⁶ with some modifications. Primary mouse endothelial cells (from mutants or ephrin-B2^{lox/lox} as a control) were blocked at 37 °C for 10 min in blocking solution consisting of DMEM, 2% (w/v) bovine serum albumin and 4% (v/v) donkey serum (Jackson ImmunoResearch). Anti-Flk1 primary antibody (R&D, 1:40) in the blocking solution was incubated with cells at 37 °C for 20 min. After two washes with warm D-PBS + Ca²⁺/Mg²⁺, cells were stimulated with recombinant human VEGF₁₆₅, pre-clustered EphB4-Fc or human Fc in endothelial medium at 37 °C for 30 min, and fixed with 4% PFA in PBS at 4 °C for 30 min. Surface receptors (green) were detected by incubation with Cy2-conjugated secondary antibodies (Jackson ImmunoResearch, 1:200) without permeabilization for 2 h at room temperature. After three washes with PBS, cells were permeabilized for 30 min with ice-cold PBS containing 0.2% Triton X-100, 2% (w/v) bovine serum albumin and 4% (v/v) donkey serum, and Cy3-conjugated secondary antibody (Jackson ImmunoResearch, 1:200) was incubated with the cells for 1 h at room temperature to visualize internalized receptors. A digital camera (SpotRT; Diagnostic Instruments) attached to an epifluorescence microscope (Zeiss) equipped with a ×63 objective (Plan-Apochromat, Zeiss) was used for imaging. Quantitative measurements based on fluorescent intensities were performed using MetaMorph software (Molecular Devices). Quantification of four independent experiments with more than 20 cells per condition was performed by analysing percentages of internalized receptors (red fluorescence) from total amount of receptors (green fluorescence + red fluorescence). Student's *t*-tests were used to assess statistical significance of the differences between measurements.

Cell surface biotinylation assay. The assay was performed as described²⁶ with minor modifications. To label surface proteins, MECs from ephrin-B2ΔV or wild-type mice as a control were incubated with 0.5 mg ml⁻¹ EZlink-NHS-SS-Biotin (Pierce) in D-PBS buffer with 1 mM MgCl and 0.1 mM CaCl at 37 °C for 5 min. Cells were washed and stimulated with 4 μg ml⁻¹ EphB4Fc or control hFc in D-MEM medium at 37 °C for 10–60 min as indicated. Biotin bound to proteins which remained on the cell surface was cleaved out by incubation with 46 mg ml⁻¹ reduced L-glutathione (Sigma) in 150 mM NaCl for 30 min at 4 °C.

Glutathione was then neutralized by incubation with 9.2 mg ml⁻¹ iodoacetamide (Sigma) in D-PBS buffer with Ca²⁺ and Mg²⁺ for 15 min at 4 °C. Cells were lysed and processed as described for tissue biotinylation.

Live tissue surface biotinylation assay. Acute cortical slices (400 µm thick) from ephrin-B2ΔV or wild-type littermates as a control were prepared from brains of P8–9 mice using a custom-made slicer. Slices were kept in artificial cerebrospinal fluid (ACSF; 124 mM NaCl, 3 mM KCl, 1.25 mM KH₂PO₄, 2.5 mM CaCl₂, 2 mM MgSO₄, 26 mM NaHCO₃, 10 mM glucose, saturated with 95% O₂ and 5% CO₂) for 1–2 h at room temperature. To label surface proteins, slices were incubated on ice with EZlink-NHS-SS-Biotin (Pierce) at a concentration of 0.5 mg ml⁻¹ ACSF for 1 h. After two washes with ACSF, 10 µg ml⁻¹ EphB4Fc or control hFc proteins were applied to the slices. Stimulations were performed for 1–1.5 h at room temperature. Remaining surface biotin was stripped out by incubation with 46 mg ml⁻¹ reduced L-glutathione (Sigma) for 30 min on ice. Glutathione was subsequently neutralized by incubation with ethanolamide (0.9 µl ml⁻¹ ACSF) on ice for 30 min. Slices were washed twice with ACSF and cells were lysed with NP-40 lysis buffer (see immunoprecipitation). Equal amounts of proteins from each sample were incubated with Neutravidin sepharose (Pierce) on a rotating wheel overnight at 4 °C. Beads were washed three times with lysis buffer and boiled at 95 °C in SDS sample buffer before proceeding with western blot analysis.

Immunofluorescence. After stimulation, endothelial cells from mutant mice or ephrin-B2^{lox/lox} mice as a control were fixed in 4% paraformaldehyde in PBS at 4 °C for 30 min. Cells were incubated with NH₄Cl for 10 min at room temperature and blocked with PBS containing 2% (w/v) bovine serum albumin and 4% (v/v) donkey serum for 1 h at room temperature. Triton X-100 (0.2%) was added to the blocking solution when permeabilization was required. Cells were incubated with primary antibody in blocking solution for 1 h at room temperature, washed three times with PBS and incubated with secondary antibody for 1 h at room temperature. Concentrations of antibodies used were as follows: rabbit anti-Tyr 1175 VEGFR2 (Cell Signalling Technology) 1:200, rabbit, goat anti-VEGFR2 (R&D Systems) 1:100, donkey anti-hFc (Jackson ImmunoResearch) 1:100. Vectashield mounting medium containing DAPI was used to mount samples. A similar protocol was applied for immunofluorescence of whole-mount retinas with variation in incubation times. EphB4-Fc and ephrin-B2-Fc fusion proteins were used at a final concentration of 5 µg ml⁻¹. Rabbit anti-GFAP (DAKO), and Cy5-conjugated goat anti-hFc (Jackson ImmunoResearch) were used at dilution of 1:70 and 1:100, respectively. For Tyr 1175 quantification, three independent experiments with 24–45 cells per condition were performed by analysing the percentage fluorescence intensity in every mutant versus total intensity in the control. Student's *t*-tests were used to assess statistical significance of the differences between measurements.

Immunoprecipitation and immunoblotting. Experiments were performed as described²⁶ with some modifications. MECs isolated from ephrin-B2ΔV or wild-type mice as a control were starved for 4 h, 80 µM dynasore was added for the last 2 h, followed by stimulation with recombinant human VEGF₁₆₅. Neonatal mouse brains or MECs were lysed with NP-40 lysis buffer (50 mM Tris HCl buffer, pH 7.5, 1% NP-40, 150 mM NaCl, 10 mM sodium pyrophosphate, 20 mM NaF, 1 mM sodium orthovanadate and 1% complete protease inhibitor cocktail (Roche)), centrifuged at 15,700g for 10 min, and supernatants were collected. The samples were pre-incubated with protein G-Sepharose beads (Pharmacia) for 30 min at 4 °C. Beads were removed by centrifugation at 1,500g. For immunoprecipitation, supernatants were incubated with 40 µl protein G-Sepharose beads pre-bound with 4 µg anti-flk1 antibody (R&D systems) or 5 µg EphB4-Fc or hFc for 2 h at 4 °C. Protein samples (from total lysates or immunoprecipitation) were separated in 7.5% SDS-polyacrylamide gel electrophoresis and transferred to 0.45-µm nitrocellulose membranes (Schleicher & Schuell). Anti-pTyr 951, anti-pTyr 1054, anti-pTyr 1175, anti-pTyr 1212 and anti-pSer Akt antibodies (Cell Signalling Technology, 1:1,000) were used to detect the level of phosphorylated VEGFR2 at the tyrosine residues indicated or activated Akt. Membranes were incubated in stripping buffer (5 mM NaH₂PO₄, 2% SDS and 0.02% β-mercaptoethanol) at 60 °C for 30 min and the amounts of VEGFR2 or Akt were assessed with anti-flk1 antibody (clone A-3, Santa Cruz Biotechnology, 1:200) or anti-Akt (Cell Signalling Technology, 1:1,000). Western blots are representative of five independent experiments.

Generation of murine astrocytomas. High-grade syngenic astrocytomas were generated by immortalizing astrocytes with SV40 large T-antigen/V-12H-ras. This tumour model has already been successfully used to reveal the functional significance of HIF and VEGF in tumour angiogenesis and progression²⁸. Briefly,

primary astrocytes were isolated from P1–2 mice in CD1 background and plated in non-coated polystyrene culture flasks. Astrocytes were purified by shaking the flasks on a rotator at 250 r.p.m. at 37 °C for 2 days to detach all other neuronal cells. Cells were washed and the medium was changed every day. After confirmation of purity by staining with anti-GFAP antibody, astrocytes were stably co-transfected with SV40 large T-antigen expression construct and the pEYFP-N1 plasmid (Clontech) by electroporation with a Nucleofector Kit (Amaxa). After selection in medium containing 300 µg ml⁻¹ geneticin (Gibco) for 2 weeks, resistant colonies were pooled and infected with a retrovirus containing the H-RasV12 oncogene (Addgene). Colonies grown in selection medium containing 2 µg ml⁻¹ puromycin (Sigma-Aldrich) were pooled. Expression of SV40 large T-antigen and H-RasV12 proteins was confirmed by immunoblot analysis with the corresponding antibodies (Calbiochem).

Tumour transplantation. CD1 ephrin-B2ΔV and control littermate or C57B/BL6 ephrin-B2^{ΔEC} and control littermate (ephrin-B2^{WT/loxP}Cre⁻ treated with tamoxifen) mice were anaesthetized and placed into a stereotaxic apparatus (Kopf Instruments). A burr hole was made 2 mm left of the sagittal suture and 0.5 mm anterior to the bregma using a dental drill 0.7 mm in diameter. For transplantation, 5 × 10⁴ CD1 astrocytoma cells (see above) or C57B/BL6-Gl261 astrocytoma cells were resuspended in cold, CO₂-independent medium and slowly injected at a depth of 3.5 mm from the dura using a 2.5-µl Hamilton microsyringe with an unbevelled 33G needle. Mice were maintained until the development of neurological symptoms. Two separate transplantation experiments were performed with independently generated CD1 astrocytoma lines (*n* = 7–11). Endothelial-cell-specific function of ephrin-B2 in Gl261 intracranial tumour growth was assessed in mice with an endothelial-specific tamoxifen-inducible ephrin-B2 loss-of-function (ephrin-B2^{ΔEC}; *n* = 8–9). Tumour-bearing mice were injected with 100 µg biotinylated tomato lectin (Vector Laboratories) retrobulbarly, 5 min before cardiac perfusion with 4% PFA in PBS. Tumour volume was determined by tracing the tumour area using the semi-automated stereological system Stereo Investigator 4.34 (MicroBrightField) and a Carl Zeiss Axiophot microscope, equipped with a Hitachi HV-C20A camera. Series of every twelfth section (480-µm interval) throughout the brain were analysed. For subcutaneous tumour injections, CD1 ephrin-B2ΔV and control littermates were anaesthetized, shaved and 2 × 10⁶ CD1 astrocytoma cells resuspended in PBS/Matrigel were injected in a total volume of 200 µl into either flank of the mice. Tumour-bearing animals were maintained for 21 days until tumours exceeded a volume of 800 mm³. Tumours were frozen in Tissue-Tek for further histological analysis (*n* = 15–17). Statistical comparisons of values were made using the Student's *t*-test. Statistical significance was defined as *P* < 0.05.

Immunohistochemistry. Tumour samples were frozen and cut into 40-µm (intracranial tumour) or 8-µm (subcutaneous tumour) sections. For haematoxylin and eosin staining, they were first stained with Mayer's haematoxylin (10 min) and then counterstained with alcoholic eosin for 2 min. For immunohistochemical studies, free-floating (intracranial tumour) or mounted (subcutaneous tumour) sections were washed in PBS. Endogenous peroxidase was neutralized with 0.6% H₂O₂ in PBS for 30 min. After washing again in PBS, sections were mounted on microscope slides and dried for 3 h at room temperature (intracranial tumour). Antigen retrieval was performed for 10 min in Tris-EDTA buffer, pH 8.0, in a steamer. Sections were blocked with 20% normal goat serum (NGS)/0.01% Triton in PBS for 1 h. For CD34 staining, sections were blocked with 5% bovine serum albumin (BSA)/0.01% Triton for 1 h. Subsequently a second blocking step was performed using 20% NGS/0.01% Triton in PBS for 1.5 h. The sections were then treated overnight at 4 °C with CD34 primary antibody (1:100, clone MEC14.7, Abcam) in 10% NGS/0.01% Triton in PBS. After washing in PBS, sections were incubated with secondary antibody peroxidase-conjugated goat anti-rat IgG, and diluted 1:100 in 10% NGS/0.01% Triton in PBS for 1 h. After a PBS wash, visualization was performed using the CSA II, Biotin-Free Catalysed Amplification System (Dako) according to the manufacturer's instructions. After washing in PBS, sections were counterstained in haematoxylin for 8 min and mounted in Aquatex (Merck). Vessel density was quantified by measuring blood vessel area stained with CD34 in ten randomly chosen optical fields per tumour. Student's *t*-tests were used to assess statistical significance of the differences between measurements.

32. Grunwald, I. C. *et al.* Hippocampal plasticity requires postsynaptic ephrinBs. *Nature Neurosci.* **7**, 33–40 (2004).

33. Lauterbach, J. & Klein, R. Release of full-length EphB2 receptors from hippocampal neurons to cocultured glial cells. *J. Neurosci.* **26**, 11575–11581 (2006).